THE SOLAR SUBMILLIMETER TELESCOPE POINTING MODEL

Myrna Yoshie Kagohara
Carlos Guillermo Giménez de Castro
Universidade Presbiteriana Mackenzie (UPM)

ABSTRACT

Professional telescopes require high pointing precision to make observations. To achieve this goal, they have sophisticated servomechanisms to move a heavy structure with an angular precision that must be of the order of the arcsec. Nonetheless, pointing errors to the real position are found in any telescope. These errors are mitigated applying corrections to the pointing system by the construction of the so-called Pointing Model. In this article is presented a long run analysis of the Solar Submillimeter Telescope (SST) pointing errors and the pointing model used to reduce them. It was used more than 20 years of observational data and the Tpoint commercial software to obtain different sets of pointing model parameters, looking to reduce the pointing errors. It was found that *ante meridiem* (AM) pointing model is different from the post meridiem (PM) one. Furthermore, errors are higher in the North-South direction, indicating a higher mechanical stress. It provides recommendations for improving the telescope pointing.

Keywords: Pointing model. Radiotelescope. Solar Map.

1 INTRODUCTION

Solar observations are very important for the study of Physics, Astronomy, Cosmology, Chemistry, high energy phenomena, and so on. Full-Sun observations can provide data for studies on solar wind (Brooks; Ugarte-Urra; Warren, 2015) and solar

radius (Menezes, 2017), for instance. Phenomena that occur on specific regions on the solar disc, such as sunspots, active regions, and related flares, make use of observations of small-scale structures, and these observations need high absolute and relative accuracy. Thus, accurate pointing of the observational instruments is a requisite.

Considering solar flares, radio telescopes working at centimetric, millimetric, and submillimetric wavelengths are very appropriate for their study, because they allow the observation of different radiation emission mechanisms occurring on our star. This provides a deeper understanding of solar activity and, consequently, Sun-Earth relationships, which affect our planet. Some bands of the electromagnetic spectrum can be observed from the ground, and one telescope that takes advantage of this fact is the Solar Submillimeter Telescope (SST) (Kaufmann *et al.*, 2008). It is located in the Argentinian Andes, at *Complejo Astronómico El Leoncito* (Casleo), and has six detectors, operating at two different frequencies: four of them, at 212 GHz, and the remaining two, at 405 GHz, at wavelengths of 1.414 mm and 0.740 mm, respectively (Castro et al., 2018). SST has been used for observing the calm, quiescent, and active Sun, with the purpose of investigating emissions of energy and matter, helping to unveil the nature of the corona and inner layers of the Sun. Atmospheric transparency studies were also done using SST (Espinoza, 2017). Currently, the SST is not operational, and requires extensive maintenance and modernization.

It must be noted, however, that the beam size decreases with increasing operational frequencies — or decreasing wavelengths — thus, the radio telescope pointing precision must improve accordingly. Also, as solar flares occur in a relatively short time scale, stringent precision and speed requirements are imposed on these telescopes.

Real-time pointing corrections and minor adjustments of telescope structure are desirable for compensating operational deviations. In an ideal situation, the beam position would be measured with some degree of accuracy. In the case of Sardinia Radio Telescope (Poppi *et al.*, 2010), the pointing errors of its mechanical structure are measured with an accuracy of about ~1 arcsec. Moreover, both primary and secondary reflectors are fitted with active surfaces, allowing faster and more accurate pointing performance.

SST, in turn, is not fitted with such high-end systems. There is no way to measure, in real time, the pointing error caused by the deformations of the mechanical structure due to gravity and movement inherent to the operation at relatively high speeds. For correcting systematic errors, however, it makes use of a well-establish method called pointing model, explained later in this article. Although it allows *a posteriori* pointing calibration, it is widely adopted, and provides satisfactory accuracy for amateur and professional telescopes. High-end equipment also takes profit from this method, further increasing observational accuracy.

This article describes the studies of SST pointing calibration using pointing models, based on works from Meeks *et al.* (1968) and Mangum *et al.*, (2006). Tpoint, a telescope pointing analysis system, which was deployed on SST in 2006, is the chosen tool for analyzing the pointing performance of the SST, based on the large amount of observational data produced by the telescope from 1999 to 2019.

2 A REVIEW OF TELESCOPE POINTING

2.1 Observing the Sky

No matter the motivation, observations of the sky start from knowing where to look at, *i.e.*, a direction must be specified. This is done using *celestial coordinates*, which make use of the notion of an arbitrarily large *celestial sphere* having the Earth at its center, as shown in Figure 1. The points on its surface have a one-to-one correspondence with observational directions (Thorstensen, between 1991 and 2001). The celestial sphere is a concept that establishes a solid foundation for Astronomy.

This way, the representation of directions of the objects in the sky, no matter their distance from Earth, is reduced to the problem of getting coordinates that represent the points on the surface of this sphere. Making a generalization of geographical notions of latitude and longitude, and defining the North Celestial Pole as being the point at which the north part of the Earth's axis of rotation intercepts the celestial sphere, the *Equatorial System of Coordinates* is defined (see Figure 1). The celestial equator ends up parallel to the Equator of the Earth, and it allows to define coordinates of this system, namely *declination* (δ) and *right ascension* (α).

Just as any location on the surface of the Earth can be defined by its latitude and longitude, the position of any object in the sky is defined by its values for declination and right ascension (roughly speaking, its "celestial latitude" and "celestial longitude," respectively). The zero point for right ascension is the vernal equinox (γ), and for declination, the Celestial Equator.

Given that the right ascension and declination of a given celestial target are enough to uniquely define its position, an idea arises: by fitting a telescope with a *mount* having two drive shafts, perpendicular to each other, and pointing one of them to the Celestial Pole (*i.e.*, aligning it with the Earth's axis of rotation), it suffices to rotate this (vertical) shaft to an angle equal to the right ascension of the desired object, and the other (horizontal) shaft to the object's declination, to aim your telescope. Basically,

this is how a telescope with an *equatorial mount* works. To keep the telescope properly targeted to the object, all you have to do is to keep the vertical shaft (or right ascension shaft) moving in the opposite direction of the rotation of the Earth, at the same rate, and leave the other shaft locked at the object's declination.

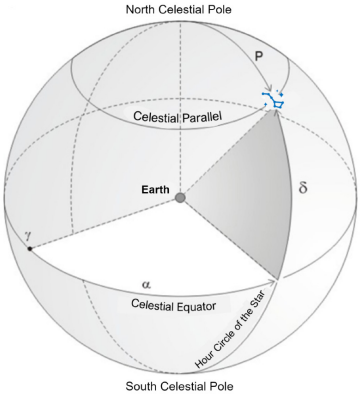

Figure 1 Equatorial System of Coordinates (γ = vernal equinox; δ = declination; α = right ascension)

Source: Santiago (2010); translated by the authors.

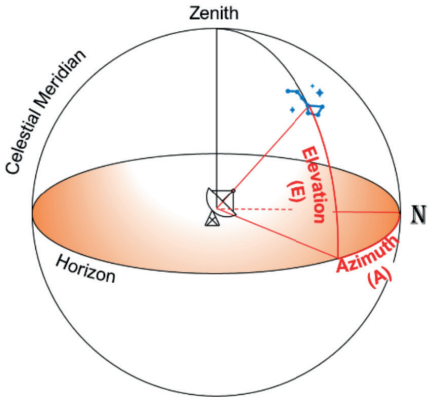

Figure 2 Horizontal System of Coordinates, where N = Geographical North; A = Azimuth; E = Elevation

Source: The authors (2022).

Constructive issues, however, come into play. Telescopes with equatorial mounts face significant engineering challenges. Tucker (2020) mentions asymmetric mass distribution and more weight, and this combination implies more stress on structural components. Moreover, the more stringent speed requirements demand higher gear stiffness, which can be attained with larger gears.

With the usage of advanced microprocessor systems for steering telescopes, cheaper and lighter *altazimuth mounts* are a good choice. They have two drive shafts, perpendicular to each other, allowing the telescope to rotate about a vertical axis and a horizontal axis. This arrangement is much easier to design and build, because the moving loads do not change their orientation to the bearings, which results in less load on them. However, their usage was difficult without today's motion controllers, since the tracking of a celestial target required the shafts to be moved simultaneously, at different rates, and the rotating field of view demanded compensation.

Using an altazimuth mount, movement control of the telescope is based on the *Horizontal System of Coordinates*, shown in Figure 2. It is a spherical-polar coordinate system, similar to the Equatorial System of Coordinates, but its center is located at the

observer's location, rather than the center of the Earth. The coordinates of the celestial object in this system can be provided directly to the drives of the shafts for elevation and azimuth axes for pointing.

Santiago (2010) explains the geometrical relationship between Equatorial and Horizontal coordinate systems, combined with the Earth's movement in space, is the basis for converting the coordinates of a given object in the sky from one system to another.

2.2 Radiotelescopes and solar observations

Figure 3 shows the schematic of a typical radiotelescope — in this case, one of the radio antennas of the ALMA observatory. Its basic elements are listed in red, and an outline of its operation is shown in blue.

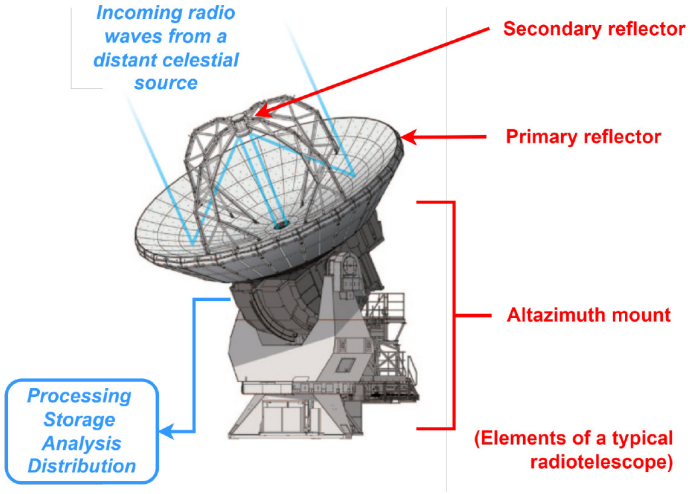

Figure 3 Radiotelescope

Source: National Astronomic Observatory of Japan (2012); adapted by the authors

The *altazimuth mount* steers the antenna in the desired direction. When the incident electromagnetic waves from the target hit the *primary reflector*, they are reflected and concentrated into the reflector's geometric focus. Specifically for the

antenna in Figure 3, the focused beam hits the *secondary reflector*[1], and is redirected into the antenna's focal plane, where electronic transducers, calibrated for the frequencies of interest, detect the signal from the sky and convert it into digital data. Along with information on the position of the source of the celestial electromagnetic waves and the time of their acquisition, raw data are stored for further processing, distribution, and scientific study.

For detecting the right radiation from the sky, the location of the radiotelescope matters a lot. Figure 4 shows the so-called *atmospheric windows* for an observer on the Earth, as a function of electromagnetic wavelength. For instance, for observing X-ray sources, the detectors must be above the atmosphere, which is opaque in this frequency band. Visible light, on the other hand, can be observed on the ground, since (not surprisingly) the atmosphere is transparent to it.

There are other factors involved, such as refraction, pollution, and so on. Thus, astronomical observatories must be deployed away from interferences in the frequency band they are intended to study. Optical telescopes for night sky observations, which operate on the visible light band, must be located far from artificially illuminated sites. The highly sensible detectors of radio telescopes, in turn, suffer interference from radio-emitting devices, such as electronic wireless devices and mobile telecommunications networks and devices. Still considering the radio band, some atmospheric windows do not reach the level of the ground, and observation within the related band requires the radio telescopes to be installed at an altitude high enough to reach the window bottom.

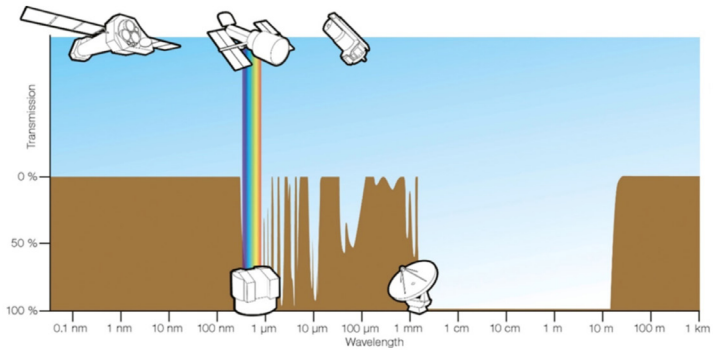

Figure 4 Atmospheric windows

Source: Condon; Ransom, 2018.

1 There are other types of altazimuth antennas without a secondary reflector, and the radiation reaches the detection instrumentation by means of different arrangements.

For creating an image from the radio observational data, not only the radiotelescope must be pointed to the object, but a scan around its position must be done, as outlined in Figure 5. This allows the collection of celestial electromagnetic radiation for an array of contiguous positions. For each position, the analog output of the electromagnetic radiation detector provides the strength of the radiation on that tiny patch of the sky. The resulting value is then converted into a digital signal, linked to its date-timestamp, and stored as a pair of numerical values. For the whole scan interval, all these pairs of radiation strength and date or timestamp are stored in a time series of data, and this can be processed for generating the radio image of the observed target using numerical calculation algorithms.

Unlike an image in visible light, which can be instantly acquired using a CCD device (which consists of an array of photodiodes), radio images are produced much later, after all the individual radiation strength values, in each of the positions of the array, are converted from analog to digital form, linked to their celestial position data and collection time, stored, and then processed to get the image (Mangum, 2015). This is because the construction of large arrays of radio-band detectors is not trivial. The smaller the spacing between scan lines, the higher the resolution of the image obtained in the observing run. For operating the antenna like this, the beam must be steerable with high precision – thus, the primary or secondary reflector, or both, must be moved fast and accurately.

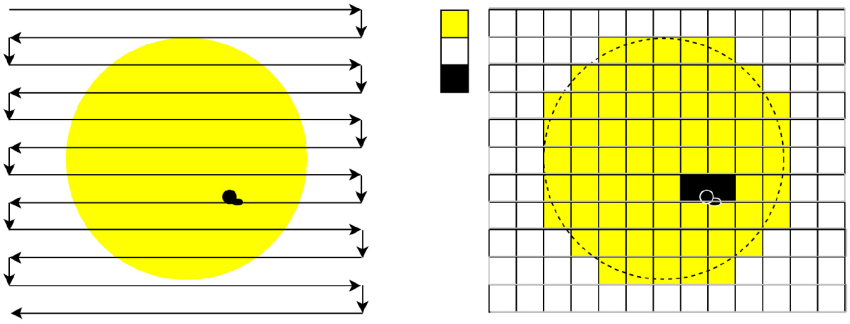

(a) Path of the radio telescope beam when scanning the Sun and the surrounding area

(b) Resulting "pixelated" image. Higher resolution images require smaller spacing between scan lines and higher sampling rate

Figure 5 Imaging scan by a radio telescope

Source: The authors (2022)

A very special target of interest in the radio band is impulsive solar flares, the most energetic phenomena in the Solar System. They result from the release of energy across the electromagnetic spectrum, from a localized area in the low corona, which occurs in a time scale of minutes (Benz, 2016). In the radio band, observation of emissions from solar flares provides information on energy release, electron acceleration and energization, and electron and energy transport. Bastian, Benz, and Gary (1998) describe two broad categories of flare observations: (i) imaging at defined frequencies, very useful, for example, in elucidating the relationship between radio, soft X-ray, and hard X-ray emissions; and (ii) broadband spectroscopic observations with no or little spatial resolution, that depend on an atmosphere model and allow the exploration of the plasma radiation from charged particles that are accelerated in the solar atmosphere and interact with magnetic fields and plasma conditions.

2.3 Antenna pointing accuracy and pointing models

The main factors that affect the pointing accuracy of a basic radio antenna, according to Gawronski (2005), are listed in Figure 6. It can be seen as a hybrid control system, with closed-loop (blue) and open-loop (red) sections. The former refers to a conventional movement control system, which sends commands for the antenna mount drives and receives the readouts of the encoders connected to the shafts, for positioning the radio telescope beam during operation. The latter shows elements that do not send feedback signals to the controller.

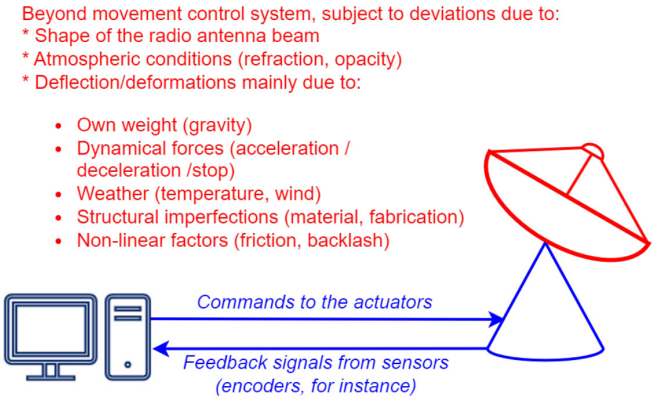

Figure 6 Antenna pointing control system

Source: The authors (2022).

Deviations in the open-loop control section are not negligible and impose significant challenges for precise observations. Considering solely the precision, it would be desirable to extend as much as possible the closed-loop control using metrology systems and deal with systematic and non-systematic deviations in real time. For instance, the Sardinia Radio Telescope (Bolli *et al.*, 2016), besides having active surfaces on the primary and secondary reflectors, is fitted with metrology systems installed on the structure and on both reflectors that provide feedback signals and allow more precise commands to be sent to the telescope actuators.

But even the most detailed and expensive telescopes suffer from external factors that cause pointing deviations. The most common resource for correcting those residual errors is the *pointing model*. Meeks (1968) describes a methodology for determining the pointing deviations using a system of equations, whose coefficients are calculated by fitting a set of observational data to them, using the least squares method. Once these coefficients are calculated, they are used to calculate the compensation to be applied to each of the shafts of the telescope mount for a more accurate pointing of the telescope. The pointing model for a large alt-azimuth antenna is derived as summarized in Figure 7. The pointing errors are supposed to be small so that the pointing error can be expressed as a linear combination of them.

The equations for pointing deviations are derived considering two reference frames: the antenna and the sky, each of them with its own system of coordinates. The antenna pointing deviation from the real position of the celestial target is determined using the equations detailed in Figure 7, then applying the Least Squares Method to a set of observational data for solving these equations.

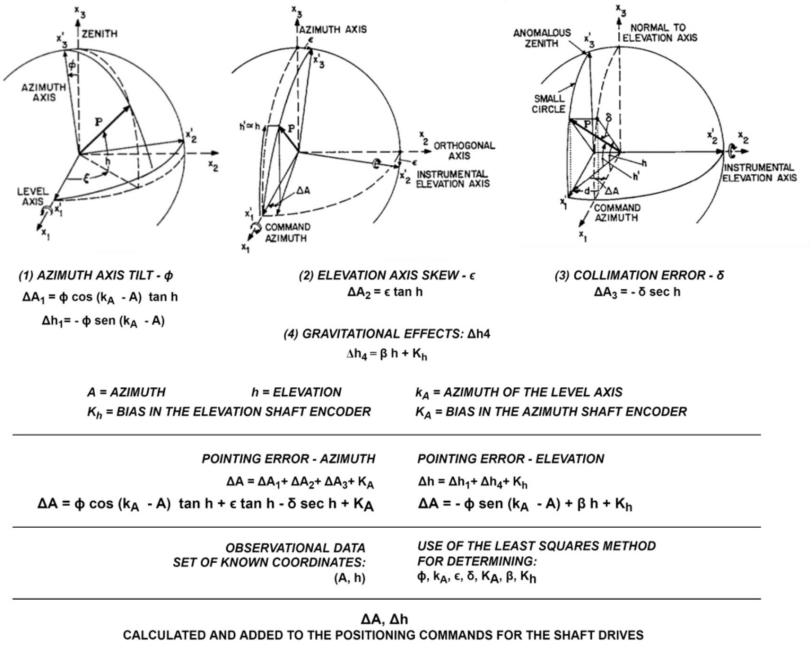

Figure 7 Pointing model calculations

Source: Meeks (1968); adapted by the authors.

Compensation of external factors, such as wind pressure and atmospheric conditions, is not included in the pointing model approach. Those factors can be compensated, for instance, with the usage of multiplicative factors applied to the processing of the observational data collected with the telescope. It is still not clear how those compensations are done.

2.4 Pointing model using tpoint for altazimuth telescopes

Similarly to the methodology described by Meeks (1968), Tpoint Software (2006) fits a pointing model for a given telescope using a set of observational data, with its own proprietary algorithm. Prototypes for ALMA antennas, for example, were validated (Mangum *et al.*, 2006) and are successfully operated using Tpoint.

Pointing deviations are described as mathematical formulae, as shown in Figure 7, and expressed in arcsec. They are used by the telescope movement control system to adjust the commands sent to the shaft drives. As described in Tpoint Software (2006),

as much as possible, the telescope pointing model should describe the physical effects, such as geometric misalignment, deflections, and so on. This allows a better understanding of which parts of the mechanical structure of the telescope are causing the pointing deviations, or if they are related to time or temperature, for instance. Then, if any systematic residual errors persist, empirical corrections can be applied. These corrections are described as harmonic or polynomial functions of the pointing coordinates.

Tpoint has a library of terms for pointing models, which can be sorted as (1) geometric (with altazimuth and equatorial subtypes), (2) flexure-related, (3) specific to some telescopes, and (4) generic (with polynomial and harmonic subtypes). A sample of these terms is given in Table 1. Note that each of them unfolds into corrections in azimuth and elevation that can be provided to the control system for a better pointing performance.

TABLE 1

Tpoint geometric coefficients for altazimuth telescopes

Coef.	Description	Effect	Correction Formula
IA	Azimuth zero-point error.	Error in the azimuth direction.	$\Delta A = -IA$
E	Elevation zero-point error.	Error in the elevation direction.	$\Delta E = +IE$
NPAE	Non-perpendicularity between azimuth axis and elevation axis.	Horizontal shifts of the image, proportional to sin (E).	$\Delta A \simeq -NPAE\tan(E)$
CA	Left-right collimation error.	Left-right shift on the sky, constant for all elevations.	$\Delta A \simeq -NPAE/\cos(E)$
AN	Azimuth axis misalignment in the NS direction.	Rotation about a horizontal axis in the EW direction equal to this coefficient.	$\Delta A \simeq -AN\sin(E)\tan(E)\Delta E \simeq -AN\cos(A)$
AW	Azimuth axis misalignment in the EW direction.	Rotation about a horizontal axis in the NS direction equal to this coefficient.	$\Delta A \simeq AW\cos(A)\tan(E)\Delta E \simeq +AW\sin(A)$

Source: The authors (2022).

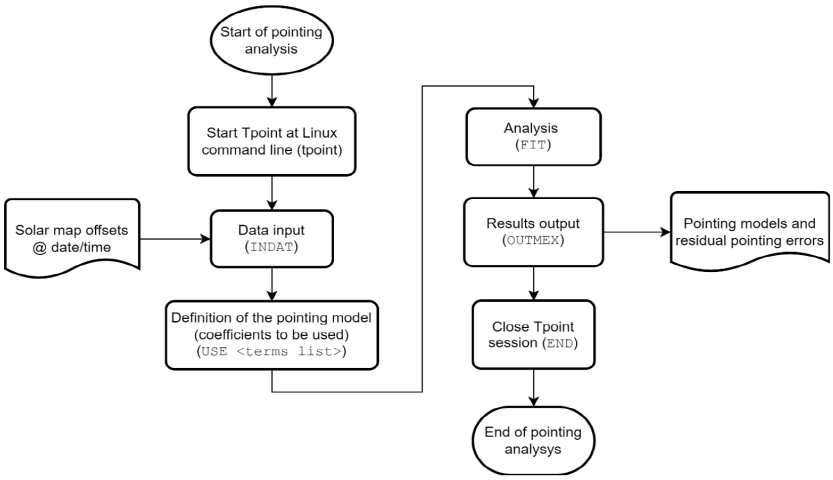

Figure 8 Tpoint operation flowchart for SST

Source: The authors (2022).

The usage of Tpoint for pointing model calculations is simple, as shown by the flowchart in Figure 8 as applied to SST. After processing a set of observational data provided as input, Tpoint calculates the pointing coefficients and residual errors in each direction, which can be provided as inputs to the telescope control system for pointing corrections. Those results can be exported in a format that is compatible with spreadsheet applications, allowing further analysis.

3 INSTRUMENTATION AND METHODOLOGY

3.1 The solar submillimeter telescope, SST

For observing the Sun at 212 GHz and 405 GHz — frequencies that were yet unexplored (Kaufmann *et al.* 2008) — SST was built and deployed at *Complejo Astronómico El Leoncito*, in the Argentinian Andes, at 2550 m above sea level. At these frequencies, atmospheric transparency allows good observations at high-altitude sites. Sample solar maps produced using SST's observational are shown in Figure 9.

SST is fitted with six radiometers that operate simultaneously. Roughly speaking, the SST is comparable to a CCD, but with fewer detectors, that opera in the radio band. Their arrangement at the telescope's focal plane is shown in Figure 10. Beams 1 to 4, in red, operate at 212 GHz; beams 5 and 6, in blue, operate at 405 GHz. Beams 2, 3, and 4 have a partial overlapping at 3 dB, allowing the comparison of antenna temperatures during solar flares for determining the emission centroid. The radiometers are housed under the main reflector backplane. The telescope is supported by an altazimuth mount with an intrinsic pointing precision of 1.8 arcsec.

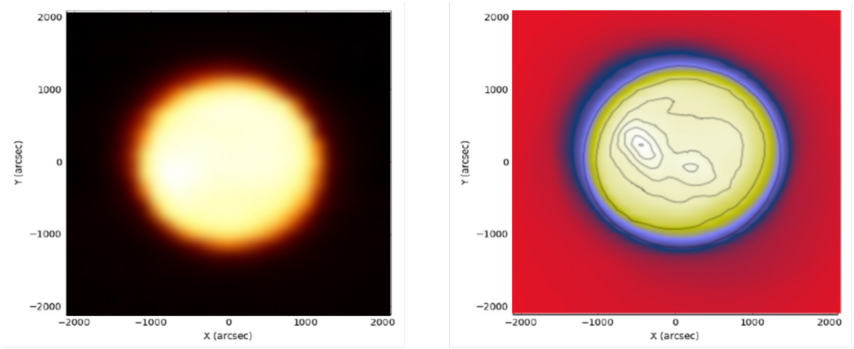

Left: Flux intensity color representation
Right: contour map for a set of relative intensities from quiet Sun level
(0.5, 0.9, 1.02, 1.04, 1.06, 1.08, 1.095).

Figure 9 Examples of solar maps acquired by the SST at 212 GHz, September 1st, 2008

Source: Menezes (2017)

Figure 11 plots the sum of the total power output of one beam during a typical scan. An automatic routine makes solar scans for mapping, followed by tipping in elevation, a solar map center scan for four minutes, and then moving to a desired active region. In this article, we will focus on solar map scans, which cover about 1° (or 3,600 arcsec) of the sky. SST makes a reading of electromagnetic radiation intensity at every 40 ms on each scan line shown in Figure 12. These lines are spaced at two arcmin gaps; the yellow circle represents the Sun disc and the smaller numbered circles, SST's beams, and their sizes.

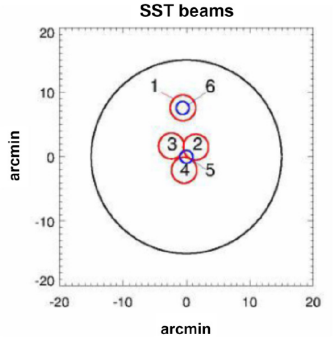

Figure 10 SST's focal arrangement of beams

Source – Kaufmann *et al*. (2008).

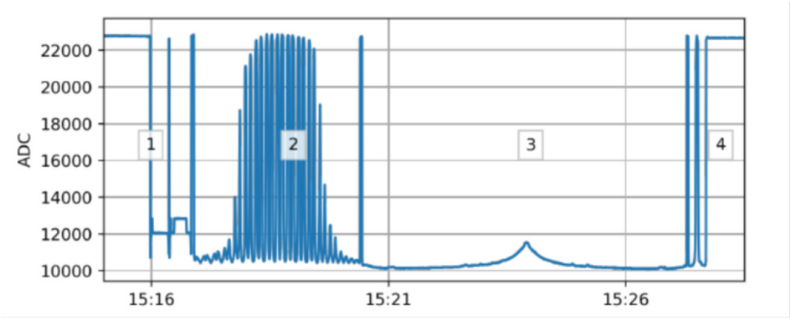

1. Temperature calibration
2. Solar map scan
3. Atmospheric opacity (τ) scan
4. Scan of the Sun map center, followed by a scan on a special region of interest (usually an active region on the Sun).

Figure 11 A typical SST scan

Source: Menezes (2017); translated by the authors.

For each scan line, SST readings are processed into a time-intensity plot, like the one shown in Figure 13. The background radiation level is shown as a blue line, and the quiet Sun level, in green. For determining the solar radius, Menezes (2017) set the middle point between background and quiet Sun levels as the value for the solar limb. After processing all scan lines, a circumference is interpolated through the limb points (see Figure 14).

When its center is different from (0,0), SST pointing has a deviation. This article aims to study ways to compensate it and, possibly, provide insights into how to eliminate it, by using pointing models. However, Menezes (2017) explains that a significant amount of calculated solar maps have been discarded during their work, mostly due to instrumental errors. This has an impact on the study of SST pointing accuracy.

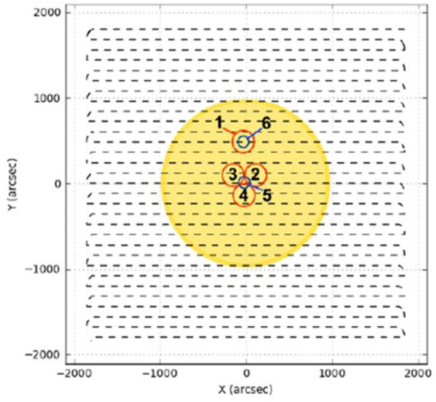

Figure 12 SST scan path for acquisition of solar maps

Source: Menezes (2017).

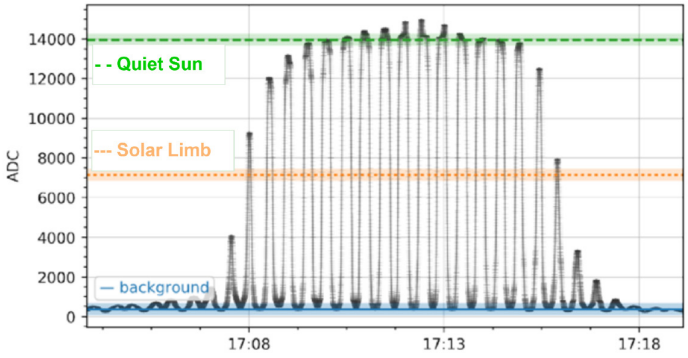

Figure 13 Solar flux collected during SST scans on January 9, 2008, showing the background, limb, and quiet Sun levels

Source: Menezes (2017); translated by the authors.

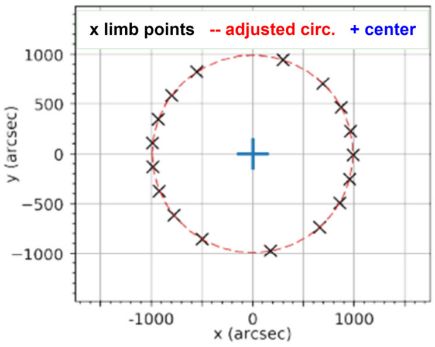

Figure 14 Limb coordinates and the interpolating circumference

Source: Menezes (2017); translated by the authors.

3.2 POINTING MODELS FOR SST USING TPOINT

The method described in Meeks (1968) was applied for SST calibration in its first version. In November 2006, an upgrade was made (Kaufmann *et al.*, 2008) for improvements of the main reflector and the introduction of Tpoint for pointing calibration, similar to the approach described by Mangum *et al.* (2006). On this occasion, the Tpoint software suite was deployed, resulting in better pointing accuracy, as detailed later in this article.

In his work, Menezes (2021) collected and reduced SST data from its first light to 2019 and obtained solar maps and their offsets of the map center from the effective target of the telescope, as described in the previous section. Based on these data, SST pointing was analyzed for data spans equivalent to seasons of the year. A pointing model was calculated for the observational data collected in each season, and residual pointing errors could be determined. Solstice and equinox dates provided by Nasa Goddard (2020) were used as limits for these time spans. The analysis process is described in Figure 15.

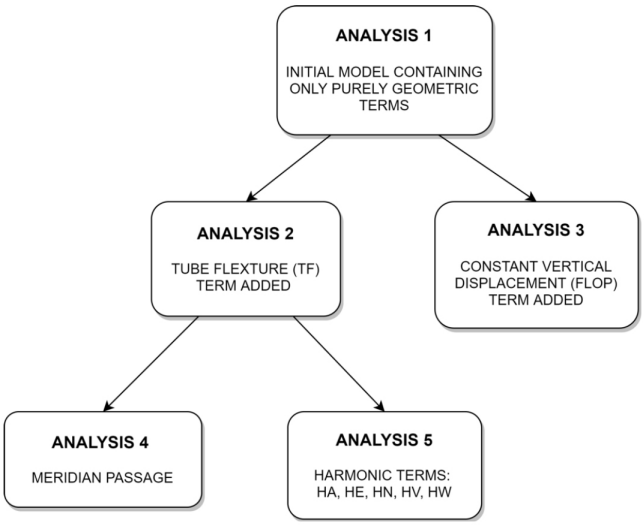

Figure 15 Analysis process of pointing models and their effects on the SST pointing accuracy

Source: The authors (2022).

Aiming for future application of the results of this work to SST operation and given that the 405 GHz receivers have reached the end of their work life, the study was initially based on observational data for 212 GHz receivers. It consisted of five analyses, shown in Figure 16, and for each of them, a specific set of pointing terms has been used. In Analysis 1, using only geometrical terms, a seasonal analysis was made from the first light in 1999, to the summer solstice of 2019.

Tpoint terms selected for use are shown in Table 1, in the previous section. CA and IE are applicable to each of the SST's channels, and the remaining terms (IA, NPAE, AN, and AW) are applicable to the telescope mount, *i.e.*, to the SST. Still referring to Figure 16, Analyses 2 to 5 use variations from this initial model; Table 2 describes the additional terms used in the detailed analysis.

TABLE 2

Terms selected for detailed analyses, applicable to the SST as a whole

Term	Description and effects
TF	Flexure of the telescope tube, supposing that its behavior can be modeled using Hooke´s Law.
FLOP	Constant vertical displacement.
HA_ _	Group of harmonic terms for empirical correction in azimuth, which are proportional to sine/cosine of elevation/azimuth.
HE_ _	Group of harmonic terms for empirical correction in elevation, which are proportional to sine/cosine of elevation/azimuth.
HN_ _	Group of harmonic terms for empirical correction that tilts the azimuth axis in the N-S direction, which are proportional to sine/cosine of elevation/azimuth.
HV_ _	Group of harmonic terms for empirical correction that changes the perpendicularity error between elevation and azimuth axis, which are proportional to sine/cosine of elevation/azimuth.
HW_ _	Group of harmonic terms for empirical correction that tilts the azimuth axis in the E-W direction, which are proportional to sine/cosine of elevation/azimuth.

Source: the authors (2022).

4 RESULTS AND DISCUSSIONS

For each season, in each analysis, a pointing model was determined for the selected terms. A total of 780 pointing models was calculated, and a sample of those models can be seen in Table 3. Tpoint also provided, for each model, sets of RMS values for N-S, E-W, left-right, up-down directions, and for the whole sky. The pointing performance is based on the analysis of such RMS values.

Figure 16 shows the results obtained after analyzing the SST data using the initial model – with purely geometric terms — from 1999 to the summer solstice of 2019. It can be seen that the residual errors in N-S and up-down directions account for most of the total RMS.

From the first light (1999) to 2005, SST's pointing system was based on the methodology described by Meeks (1968). In 2006, the telescope was repaired and upgraded, and Tpoint was deployed for pointing calibration. Figure 17 shows that the pointing accuracy and repeatability improved. So, for further analysis, data acquired before the summer solstice of 2006 were not used.

In this study, calculations of ephemerides and date/time were based on International Earth Rotation and Reference Systems[2] (IERS) Service tables. From 2017, the observational data was out of the range of these tables[3], and there was the possibility of positional errors of arcsec of magnitude. Then, data after the summer solstice of 2016 were not used for further analysis as well.

TABLE 3

Sample of pointing term values calculated for each season (in arcsec), using Tpoint, for observational data of 2007, in Analysis 2 (*i.e.*, for a model using IA, IE, NPAE, CA, AN, AW, and TF)

TIMESTAMP	IA	IE ch1	IE ch2	IE ch3	IE ch4	NPAE	CA ch1	CA ch2	CA ch3	CA ch4	AN	AW	TF
2007-03-20	9.4758	9.4368	2.4782	8.515	6.1169	-20.4925	-0.4737	0.0587	-2.493	0.6381	-13.9908	1.6529	13.4257
2007-06-21	-3.3199	-0.8681	-11.5224	-4.8372	-8.0468	7.7253	1.0087	0.7933	-0.9656	0.8209	-14.984	-0.5118	-3.3705
2007-09-23	-10.3444	-1.6008	-11.3749	-6.4269	-13.0287	-15.3076	20.8159	16.8276	19.3045	17.9882	-6.9062	2.0136	-14.8578
2007-12-22	-31.7922	5.067	-4.3188	-0.5485	-4.4887	-32.708	41.5818	43.3823	43.4648	45.7993	-5.5484	-1.6895	-5.2775

Note: These term values do not follow any evolution trend individually; rather, what changes in a traceable way is the pointing deviation of the telescope in each direction.

Source: The authors (2022).

So, using the data in the range of interest shown in Figure 16, further analysis runs (Analyses 2 to 5, in Figure 16) were made with the introduction of FLOP (constant vertical displacement) and TF (tube flexure) terms to the pointing model. The results are shown in Figure 17. Adding FLOP to the pointing model did not result in significant improvements. With the addition of TF, no significant improvement could be seen before the summer solstice of 2015. After this date, TF usage improves the pointing performance of SST. Possibly, the compensation of flexure of the telescope became necessary only after the wear of the equipment due to aging.

2 https://www.iers.org/IERS/EN/Home/home_node.html

3 An alternate data source should have been used, but this would require changes to the SST control software that have not been implemented by the time of data acquisition.

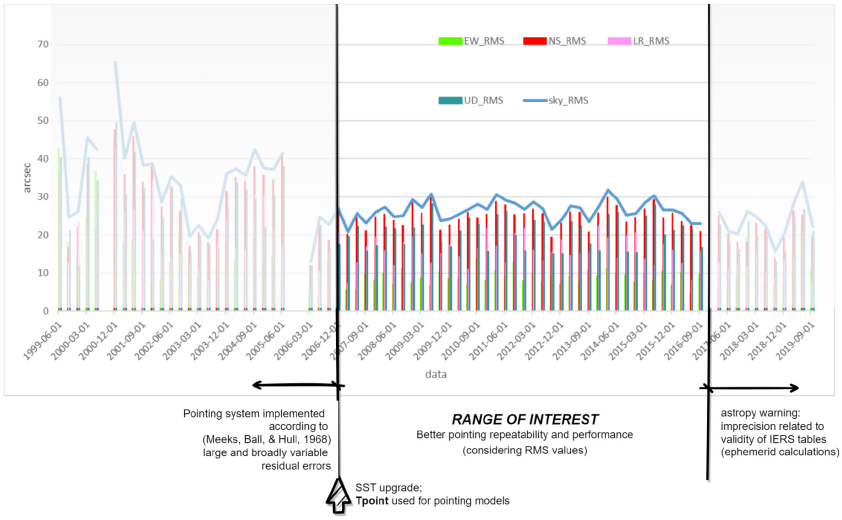

Figure 16 RMS for the whole sky and for each direction for the initial pointing model (purely geometrical terms) applied to the solar maps from 1999 to the summer solstice of 2019

Source: The authors (2022).

A further investigation in the same range of interest dealt with separate sets of observations before and after the meridian passage (approximately 15 UTC at the Casleo site) – AM and PM models. Figure 18 shows that the RMS values for AM and PM models for a given set of maps are somewhat different, providing indications that using separate models for AM and PM observations could produce more accurate pointing. It can also be noted that PM values follow the general trends of whole-day models, which could be a sign of a bias in the range of observations, with more PM data available than AM data.

Table 4 shows values for average, minimum, and maximum values of residual pointing errors from the seasonal analysis, using several types of correction factors (linked to Tpoint pointing terms). The values for residual errors (RMS) for the whole sky vary from 20.8 to 31.8 arcsec for pointing models calculated for the entire day, with standard deviations of 2.58 to 2.67 arcsec, respectively. For AM and PM models, standard deviation values are remarkably larger than those for models calculated for the entire day.

Table 5 shows the percentual values and statistical parameters of the variations of RMS values from the basic model. On average, the pointing model used in Analysis 2, which applies a correction related to a flexure modeled according to Hooke's law (parameter TF). with additional correction in the N-S direction (HN-type harmonic parameters), results in the lowest residual pointing errors.

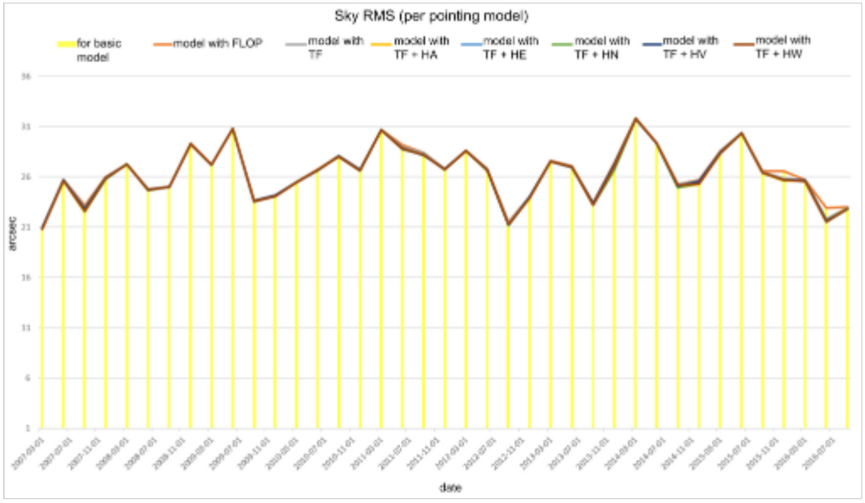

Figure 17 Consolidated graphs – all day observations considered for pointing model calculations

Source: The authors (2022).

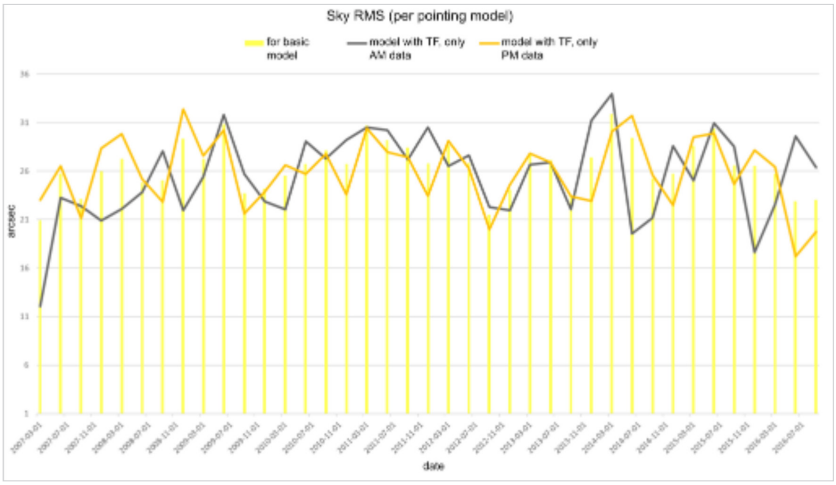

Figure 18 AM/PM separate models with TF

Source: The authors (2022).

TABLE 4

Statistical parameters of sky RMS values for each pointing model (in arcsec)

	Sky RMS for basic model	Sky RMS for model w/ FLOP	Sky RMS for model w/ TF	Sky RMS for model w/ TF+HA	Sky RMS for model w/ TF+HE	Sky RMS for model w/ TF+HN	Sky RMS for model w/ TF+HV	Sky RMS for model w/ TF+HW	Sky RMS for AM mode=l	Sky RMS for PM model
Average	26.49	26.49	26.4	26.29	26.33	26.27	26.33	26.29	25.52	25.94
Minimum	20.94	20.94	20.94	20.91	20.93	20.85	20.91	20.8	12.07	17.2
Maximum	31.87	31.87	31.81	31.75	31.79	31.76	31.77	31.79	33.97	32.4
Std. Dev.	2.58	2.58	2.63	2.66	2.64	2.67	2.65	2.67	4.45	3.52

Note: The last two columns refer to pointing models applied separately for observational data collected before the meridian passage (AM model) and after the meridian passage (PM model) at the Casleo site, which is approximately 15UTC.

Source: The authors (2022).

5 FINAL CONSIDERATIONS

The study of SST's pointing models brought about improvement possibilities for the telescope. For instance, the models show evidence that the telescope was subject to more elastic flexure in the summer of 2015 and winter of 2016. The model that

applies a correction linked to this effect produces a pointing accuracy improvement of about 1 arcsec.

The analysis that considered the hypothesis of a constant vertical displacement (a common indication of backlash in the mount) showed that this does not affect the pointing accuracy of SST.

TABLE 5

Percentual values and statistical parameters of the differences between RMS values for each pointing model and for the basic model

	Sky RMS for model w/ FLOP – basic model	Sky RMS for model w/ TF – basic model	Sky RMS for model w/ TF+HA – basic model	Sky RMS for model w/ TF+HE – basic model	Sky RMS for model w/ TF+HN – basic model	Sky RMS for model w/ TF+HV – basic model	Sky RMS for model w/ TF+HW – basic model	Sky RMS for AM model – basic model	Sky RMS for PM model – basic model
Average	0.00	-0.09	-0.20	-0.16	-0.22	-0.16	-0.20	-0.97	-0.55
% var.	0.00	0.00	-0.01	-0.01	-0.01	-0.01	-0.01	-0.04	-0.02
Min.	0.00	-1.11	-1.15	-1.18	-1.40	-1.29	-1.40	-9.85	-5.71
Max.	0.02	0.00	-0.01	-0.01	-0.01	0.00	0.00	6.66	3.05
Std. Dev.	0.00	0.21	0.25	0.22	0.27	0.23	0.25	3.75	1.98

Note 1: The last two columns refer to pointing models applied separately for observational data collected before the meridian passage (AM model) and after the meridian passage (PM model) at the Casleo site, which is approximately 15UTC.

Note 2: Negative values show that the model specified at the table header has a lower RMS value than the basic model of this analysis.

Source: The authors (2022).

An analysis using harmonic empiric corrections showed that residual pointing errors could be reduced in all the cases but with only a 1% pointing accuracy improvement, which is not enough for deem this approach worthwhile.

Separate analyses for AM and PM observational data suggest that the usage of different calibrations for each of these periods would be valid for getting more accurate solar maps. It would be interesting to check if the difference in RMS values is due to biased data collection.

Further work on the SST pointing analysis and optimization might include the following:

- Refurbishment of the mechanical structure of the telescope mount, focusing on components and subsystems that might have effects on pointing errors in N-S and up-down directions.
- Installation of metrology systems for providing inputs to the telescope pointing system, to provide a dynamic response to deviations and improve the observational performance.

- Application of software engineering techniques and tools for organizing and optimizing the source code.
- More observation runs for further investigation on AM/PM pointing model differences, providing a balanced amount of AM and PM observational data, to check if the pointing differences found in this study are indeed due to the observation time of the day, or if they only differ that much because of biased data.
- Detailed study on the accuracy of the solar disc center calculation: the center of the Sun is the reference for all this work, thus, errors in the calculation of this data have a direct impact on the pointing accuracy. The position of the center of the solar maps is affected by several uncertainty factors, for instance, those related to the method of map extraction from the solar scans (as mentioned by Menezes, 2017), or possible effects of the beam deformation for each of the detectors in the SST focal arrangement.
- Deeper investigation of environmental issues at Casleo, such as opacity and refraction, since they have a large impact on the quality of the observational data.

O MODELO DE APONTAMENTO DO TELESCÓPIO SOLAR PARA ONDAS SUBMILIMÉTRICAS

RESUMO

Telescópios profissionais precisam ter alta precisão para fazer observações e, para isso, são equipados com sofisticados servomecanismos de movimentação de suas pesadas estruturas com precisão angular da ordem de segundos de arco. Contudo, qualquer que seja o telescópio, haverá erros no apontamento real, que são mitigados com a aplicação de correções às imperfeições do sistema de posicionamento, compondo um modelo de apontamento. Neste artigo, é apresentado uma análise de longo prazo dos erros de apontamento do Telescópio Solar para Ondas Submilimétricas (SST) e o modelo de apontamento empregado para reduzi-los. Utilizou-se mais de 20 anos de dados observacionais e o software comercial Tpoint para obter diferentes conjuntos de parâmetros de modelos de apontamento, buscando a redução do erro. Pode-se constatar que o modelo ante meridiem (AM) é diferente do modelo post meridiem (PM). Além disso, os erros são maiores na direção Norte-Sul, indicando tensões mecânicas maiores. São feitas recomendações para melhorar o apontamento do telescópio.

Palavras-chave: Radiotelescópio. Modelo de apontamento. Mapa solar.

REFERENCES

BASTIAN, T. S., BENZ, A. O., GARY, D. E. Radio emission from solar flares. *Annual Review of Astronomy and Astrophysics*, [*s. l.*], v. 36, p. 131-188, 1998. doi:10.1146/annurev.astro.36.1.131.

BENZ, A. O. Flare Observations (Review). *Living reviews in solar physics*, [*s. l.*], v. 12, n. 1, p. 1-59, 2016. doi:10.1007/s41116-016-0004-3. Access on: Dec. 16, 2024.

BOLLI, P. et al. Sardinia radio telescope: general description, technical commissioning and first fight. *Journal of Astronomical Instrumentation*, [*s. l.*], v. 4, n. 3 & 4, 550008, 2016.

BROOKS, D. H., UGARTE-URRA, I., WARREN, H. P. Full-Sun observations for identifying the source of the slow solar wind. *Nature Communications*, [*s. l.*], v. 6, 5947, 2015.

CASTRO, C. G. et al. The September 6, 2017 X9 super flare observed from submillimeter to Mid-IR. *Space Weather*, [*s. l.*], v. 16, p. 1261-1268, 2018. doi:10.1029/2018SW001969. Access on: Dec. 16, 2024.

CONDON, J. J., RANSOM, S. M. *Essential Radio Astronomy - Chapter 1 Introduction*. October 25, 2018. Available at: https://www.cv.nrao.edu/~sransom/web/Ch1.html Access on: July 26, 2021.

ESPINOZA, D. C. *Determinação da opacidade atmosférica em comprimentos de ondas submilimétricas*. 2017. Dissertação (Mestrado em Ciências e Aplicações Geoespaciais) – Universidade Presbiteriana Mackenzie, São Paulo, 2017. Available at: http://tede.mackenzie.br/jspui/handle/tede/3581. Access on September 10, 2022.

GAWRONSKI, W. Control and pointing challenges of antennas and telescopes. In: AMERICAN CONTROL CONFERENCE, 6., 2005. Pasadena. *Anais* […]. Pasadena: Institute of Technology, 2005. doi:10.1109/ACC.2005.1470558.

KAUFMANN, P. et al. New telescopes for ground-based solar observations at submillimeter and mid-infrared. *Ground-based and Airbone Telescopes II*, v. 7012, p. 70120L, 2008. Available at: https://doi.org/10.1117/12.788889. Access on September 10, 2022.

MANGUM, J. *How to make images with a radio telescope*, 2015. Available at: https://public.nrao.edu/ask/how-to-make-images-with-a-radio-telescope/. Access on: June 22, 2023.

MANGUM, J. et al. Evaluation of the ALMA Prototype Antennas. *Astronomical Society of the Pacific*, [s. l.], v. 118, n. 847, 2006.

MEEKS, M. L., BALL, J. A., HULL, A. B. The pointing calibration of the haystack antenna. *IEEE Transactions on Antennas and Propagation*, [*s. l.*], v. AP-16, p. 746-751, 1968.

MENEZES, F. M. *Raio solar em frequências subterahertz e sua relação com a atividade solar*. 2017. Dissertação (Mestrado em Ciências e Aplicações Geoespaciais) – Universidade Presbiteriana Mackenzie, São Paulo, 2017. Available at: http://tede.mackenzie.br/jspui/handle/tede/3472. Access on September 10, 2022.

MENEZES, F. M. *Influência da atividade magnética na atmosfera solar e na propagação de ejeções de massa coronal de estrelas do tipo-solar*. 2021. Tese (Doutorado em Ciências e Aplicações Geoespaciais) – Universidade Presbiteriana Mackenzie, São Paulo, 2021. Available at: https://dspace.mackenzie.br/handle/10899/28902. Access on September 10, 2022.

NASA GODDARD. *Time and date of vernal equinox*. (January 2, 2020) Available at: https://data.giss.nasa.gov/modelE/ar5plots/srvernal.html. Access on July 26, 2022.

NATIONAL ASTRONOMIC OBSERVATORY OF JAPAN. ALMA - atacama large millimeter array/submillimeter array: in search of our cosmic origins. Tokyo: Naoj, 2012. Available at: https://alma-telescope.jp/assets/uploads/2017/01/ALMApamphlet_e_2012.pdf. Access on September 10, 2022.

POPPI, S. et al. High precision pointing with the Sardinia Radio Telescope. *In*: SPIE - THE INTERNATIONAL SOCIETY FOR OPTICAL ENGINEERING, 2010, San Diego. *Anais* […]. San Diego: Ground-based and Airborne Telescopes III, 2010. doi:10.1117/12.856584

SANTIAGO, B. *Geodesic astronomy notes*. Porto Alegre: UFRGS, 2010. Available at: https://www.if.ufrgs.br/oei/santiago/fis2005/textos/equatcrds.htm. Access on July 26, 2021.

TPOINT SOFTWARE. *TPOINT – a telescope pointing analysis system* (product manual). 2006.

THORSTENSEN, J. *Coordinates, time, and the sky*. (between 1991 and 2001). Available at: https://ftp.lowell.edu/www_users/massey/Thorstensen.pdf. Access on: June 22, 2023.

TUCKER, S. *German Equatorial Mounts*. Tucson, February 29, 2020. Available at: https://starizona.com/blogs/tutorials/german-equatorial-mounts. Access on: Aug. 5, 2022.

ACKNOWLEDGEMENTS

The authors of this work want to express their gratitude for the funding provided by Instituto Presbiteriano Mackenzie, MackPesquisa Fund, Capes, and Fapesp (proc.: 20313/24155-3), for the generous financial support; and also to the operations on *Complejo Astronomico El Leoncito*, accomplished under agreement between *Consejo Nacional de Investigaciones Científicas y Técnicas de la República Argentina* and La Plata, Córdoba, and San Juan Universities, for the wealth of observational data provided for this work. Dr. Carlos Guillermo Giménez de Castro also acknowledges CNPq (grant: 307722/2019-8).

Contato
Myrna Yoshie Kagohara
myrnayk.astro@gmail.com

Tramitação
Received: 09/15/2022
Accepted: 07/27/2024